and bendings (754, 700, 542 cm^{-1}) to bridgehead deformation (451 cm^{-1}), to the "butterfly" motion (410 cm^{-1}) and to the torsions (342 and 172 cm^{-1}).

Discussion

The final force field is given in Table II. The calculated frequencies are compared with the experimental values in Table III. The average error is 0.57% or 5.55 cm^{-1}. The main contributions to the potential energy distribution are also listed in Table III together with an approximate description of the modes and with the calculated neutron intensity which is related to $\sum_H C_d^2(\lambda)$.

The valence force field of Snyder and Schachtschneider was thus a very reasonable model for norbornane, but several adjustments were necessary in order to describe the vibrations of this strained molecule.

If we compare our final constants with the original values, we find that several constants have the same order of magnitude: the stretching force constants as well as the bending constants H_γ, H_ζ and H_δ. The two constants H_δ and $H_{\delta'}$, corresponding to the two types of methylene groups (2-bridge and 1-bridge) were initially allowed to float. Since the final values were almost identical, we considered only one constant for the HCH deformations.

We find that other constants are more variable, e.g., the CCC bending force constants H_ω and H_ϕ. The values corresponding to 1-bridge and 2-bridge carbon atoms decrease, whereas they increase for the bridgehead carbon atoms (the latter atoms positions are the most deformed from a tetrahedral geometry). These CCC constants are related to the twisting force constants (H_τ, $H_{\tau'}$, $H_{\tau''}$) which have a mean value of the same magnitude as for the original model.

The interaction constants do not vary significantly except F_ϕ which has a larger value due to the major role of the bridgehead deformations. The magnitude of all the interaction force constants is reasonable and this is reflected by the values of the sums of the diagonal potential energies which are close to 100%.

Conclusion

We have shown that the low-frequency vibrations of norbornane can be assigned with certainty with the help of the NIS spectra. For the range 700–1500 cm^{-1} the NIS spectrum was also of great value as a complement to the infrared and Raman data. We have modified the valence force field of Snyder and Schachtschneider to take into account the strain of the molecule.

The force field presented in this study is of course not unique[17] because of possible assignments problems and because we have used a General Valence Force Field. However, it accounts well for the observed optical frequencies and the neutrons intensities. This new force field will be used to interpret the IR, Raman, and NIS spectra of the mono and dimethyl derivatives.

Acknowledgment. We are very much indebted to A. Chosson and A. Corne (Laboratoire de Spectroscopie Optique, Université de Savoie, Chambéry, France) for their help in recording the Raman spectra. We thank Dr. J. C. Lassègues and Dr. B. Desbat (Laboratoire de Spectroscopie Infrarouge, Bordeaux, France) for their careful reinvestigation of the infrared spectra, and Dr. Ermer for details on his calculations. Finally, we thank Professor A. Rassat for his continuous interest in this work.

Registry No. Norbornane, 279-23-2; neutron, 12586-31-1.

(17) Since this paper was originally submitted, a new molecular structure of norbornane has been published by L. Doms, L. Van den Enden, H. J. Geise, and C. Van Alsenoy, *J. Am. Chem. Soc.*, **105**, 158 (1983). This new geometry, which is derived from an extensive study of experimental and theoretical results, would slightly modify our force field. However, their set of vibrational amplitudes, from which the vibrational amplitudes are computed, is not entirely correct as we show in this paper.

Effect of Crystal Packing on the Solid-State Spectral Properties of Vicinal Diketones[1]

John I. Crowley,* Richard D. Balanson, and James J. Mayerle

Contribution from the IBM Research Laboratory, San Jose, California 95193.
Received March 21, 1983

Abstract: X-ray crystal structures are reported for six substituted benzils: 4,4′-dimethoxy (**1**), 4-ethoxy (**7**), 4,4′-diethoxy (**6**), and the meso (**4b**), racemic (**4a**), and LL chiral (**4c**) bis-4,4′-(2,2′-dimethyl-1,3-dioxacyclopentyl-4-methoxy) benzils. The syntheses of **4a**, **4b**, and **4c** are described as well as the separation of **4a** and **4b**. Crystal structure data follow. **1**: a = 21.934 Å, b = 4.064 Å, c = 15.208 Å, β = 102.11°, $C2/c$, Z = 4. **6**: a = 14.512 Å, b = 4.795 Å, c = 22.089 Å, β = 98.82°, $C2/c$, Z = 4. **7**: a = 7.577 Å, b = 14.845 Å, c = 12.153 Å, β = 97.63°, $P2/n$, Z = 4. **4a**: 10.044 Å, b = 5.339 Å, c = 22.83 Å, β = 95.84°, $P2/n$, Z = 2. **4b**: a = 22.826 Å, b = 11.067 Å, c = 9.506 Å, β = 97.03°, $P2_1/c$, Z = 2. **4c**: a = 5.390 Å, b = 10.487 Å, c = 43.985 Å, $P2_12_12_1$, Z = 4. The packing modes tend to be dominated by van der Waals close packing considerations and the preference for aligning substituted phenyl rings parallel to each other at about 3.45–3.70 Å separation. Our results afford semiquantitative support for the proposition that the solid-state color of dicarbonyl compounds is red-shifted by increased overlap and blue-shifted by decreased overlap of the carbonyls. In the case of sheets of stacked substituted benzils, the increased size of the remote substituent is accommodated in the stack by increased twisting of the carbonyls while maintaining close packing of the phenyl rings.

Introduction

The solid state colors of 4,4′-substituted benzils range from the yellow of anisil and dinitrobenzil to essentially colorless compounds. An early, erroneous explanation[2] attributed yellow colors to the presence of unsubstituted dicarbonyls while the less colored or colorless compounds were explained by substituents on the dicarbonyl chromophore which were electron donating and which "neutralized" the effect of the carbonyls. Subsequently, Leonard and associates[3] explained the variation of color as resulting from

(1) Preliminary reports of this work have been presented, in part, at the 174th National Meeting of the American Chemical Society, Chicago, IL, Aug 28–Sept 2, 1977; paper 161, Division of Physical Chemistry; 178th National Meeting of the American Chemical Society, Washington DC Sept 9–14, 1979; paper 212.

(2) Robinson, R. "Outline of an Electrochemical Theory of the Course of Organic Reactions"; Institute of Chemistry of Great Britain and Ireland: London, 1932; p 30.

0002-7863/83/1505-6416$01.50/0

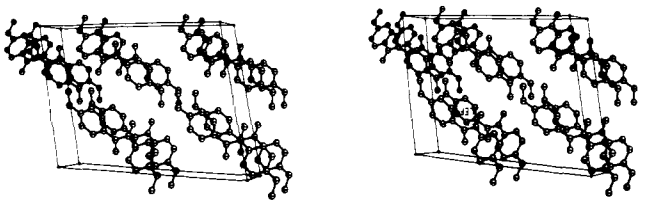

Figure 1. Stereoscopic ORTEP drawing of the unit cell of anisil, approximately along *b*. Direction of *a* is →.

solid-state packing effects since all compounds displayed the same solution spectra. No crystal structural data were presented to support this conclusion, however.

Investigation of the photophysical properties of the α dicarbonyls has focused on the intramolecular carbonyl group electronic interaction as a function of their geometrical relationship. As in the extensive studies of the photochemistry[4,5] of these compounds, biacetyl and benzil have been the almost exclusive experimental vehicles for photophysical study. Emphasis has been placed on excited-state geometry,[6-8] chiefly in solution studies. Only a limited amount of data has been gathered from solid-state configurations such as single crystals, solid matrices, or dopants in host crystals. Leonard and co-workers employed the solution UV of sterically constrained substituted benzils[3,9] and of cyclic diketones[10] to establish a semiquantitative relationship between absorption maximum and intercarbonyl angles; they also showed that crowding by ortho-substitution resulted in a nearly planar trans disposition of the dicarbonyls with an accompanying bathochromic shift of the dicarbonyl absorption maximum. Recently, application of optically detected ENDOR to a benzil single crystal has settled the question of the triplet excited-state inter-carbonyl angle, fixing it at 157°;[11] this is smaller than the trans coplanar disposition predicted from spectroscopic studies,[6-8,12] and decidedly different from the ground state value of 111° shown by X-ray diffraction.[13-15]

Lack of crystal structure data has hindered the extension of such investigations to a larger variety of substituted benzils. To our knowledge, only structures for benzil and, recently, 4,4′-dinitrobenzil[16] have been reported.

Results and Discussion

Our interest was aroused during the preparation of modified benzils required as intermediates in the preparation of nickel bisdithiolenes with increased water solubility.[17,18] An intermediate obtained on the pathway to the 4,4′-diglyceryl ether of 4,4′-dihydroxybenzil, **10**, according to Scheme I, was the 4,4′-diacetonide, **4**, in a crude yield of 80%. Workup by acetone trituration followed by recrystallization from toluene afforded colorless crystals of **4a**, (mp = 165 °C). However, combined mother liquors from several preparations afforded a second crop of crude product which could not be triturated in acetone because it was too soluble. Recrystallization of this second product from acetone/hexane yielded a new compound, **4b**, mp = 116 °C, which was almost colorless. Since these two materials had essentially identical UV, IR, and

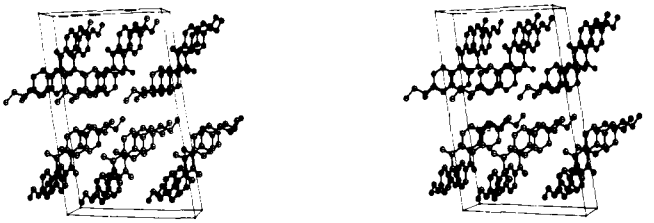

Figure 2. Stereoscopic ORTEP drawing of the unit cell of diethoxy benzil approximately along *b*. Direction of *a* is →.

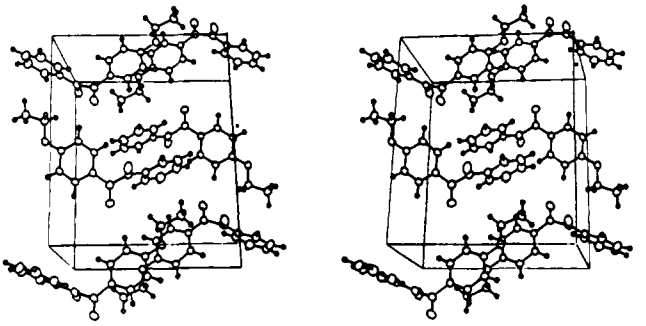

Figure 3. Stereoscopic ORTEP drawing of the unit cell of monoethoxy benzil approximately along *a*. Direction of *c* is →.

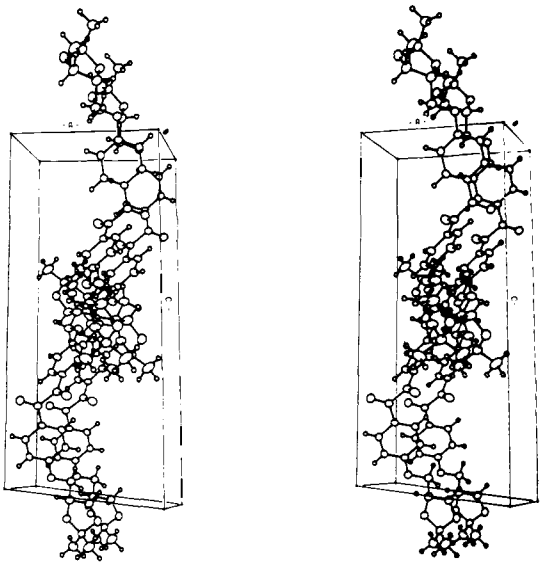

Figure 4. Stereoscopic ORTEP drawing of the unit cell of racemic bisketal benzil approximately along *a*. Direction of *a* is →.

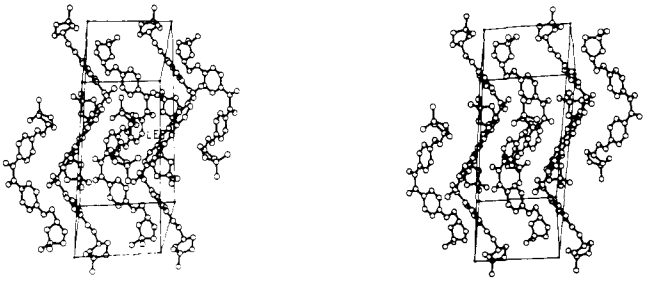

Figure 5. Stereoscopic ORTEP drawing of the unit cell of meso bisketal benzil approximately along *c*. Direction of *b* is →.

(3) Leonard, N. J.; Rapala, R. T.; Herzog, H. L.; Blout, E. R. *J. Am. Chem. Soc.* **1949**, *71*, 2997.
(4) Stevens, B.; DuBois, J. T. *J. Chem. Soc.* **1962**, 2813.
(5) Shimizu, N.; Bartlett, P. D. *J. Am. Chem. Soc.* **1976**, *98*, 4193.
(6) Evans, T. R.; Leermakers, P. A. *J. Am. Chem. Soc.* **1967**, *89*, 4380.
(7) Arnett, J. F.; McGlynn, S. P. *J. Phys. Chem.* **1975**, *79*, 626.
(8) Morantz, D. J.; Wright, A. J. C. *J. Chem. Phys.* **1971**, *54*, 692.
(9) Leonard, N. J.; Blout, E. R. *J. Am. chem. Soc.* **1950**, *72*, 484.
(10) Leonard, N. J.; Mader, P. J. *J. Am. Chem. Soc.* **1950**, *72*, 5388.
(11) Chan, I. Y.; Heath, B. A. *J. Chem. Phys.* **1979**, *71*, 1070.
(12) Bera, S. C.; Mukherjee, R.; Chowdhury, M. *J. Chem. Phys.* **1969**, *51*, 754.
(13) Brown, C. J.; Sadanaga, R. *Acta Cryst.* **1965**, *18*, 158.
(14) The angle between the benzoyl units in benzil has frequently been called 70°[12,15] in the literature and attributed to ref 13, even though these authors explicitly state that the normals to these planes are at an angle of 70°. These results are correctly cited in ref 11, although earlier errors were not referenced.
(15) Choudhuri, N. K.; El-Sayed, M. A. *J. Chem. Phys.* **1967**, *47*, 1133.
(16) Kimura, M.; McCluney, R. E.; Watson, W. H. *Acta Cryst.* **1979**, *B35*, 483.
(17) Adams, G. M.; Balanson, R. D.; Crowley, J. I.; LaVergne, D. B.; Levy, M. F.; Sachdev, H. S.; Snyder, C. D. Presented at the 14th Western Regional Meeting, American Chemical Society, San Francisco, CA, Sept 27, 1978.
(18) Adams, G. M.; Balanson, R. D.; Crowley, J. I.; LaVergne, D. B.; Levy, M. F.; Sachdev, H. S.; Snyder, C. D., to be published.

Table I. Summary of X-ray Crystallographic Results for Benzil Series

	z	ρ	a	b	c	α	β	γ	τ	space group	vol
benzil[a]	3	1.256	8.376	8.376	13.700	90	90	120	111.6	$P3,2,1$	961
anisil[b]	4	1.354	21.934	4.064	15.208	90	102.11	90	124.3	$C2/c$	1325.6
monoethoxy[b]	4	1.247	7.577	14.845	12.153	90	97.63	90	98.2	$P2_1/n$	1354
diethoxy[b]	4	1.305	14.512	4.795	22.089	90	98.82	90	95.7	$C2/c$	1519
meso	4	1.304	22.826	11.067	9.560	90	97.03	90	103	$P2_1/c$	2392
chiral[b]	4	1.257	5.390	10.487	43.985	90	90	90	94.8	$P2_12_12_1$	2486
racemic[b]	2	1.28	10.044	5.339	22.83	90	95.84	90	89.2	$P2/n$	1216
dinitro[c]	2	1.42	7.829	13.467	7.187	94.07	59.14	87.35	111.5	$\bar{P}1$	646

Scheme I

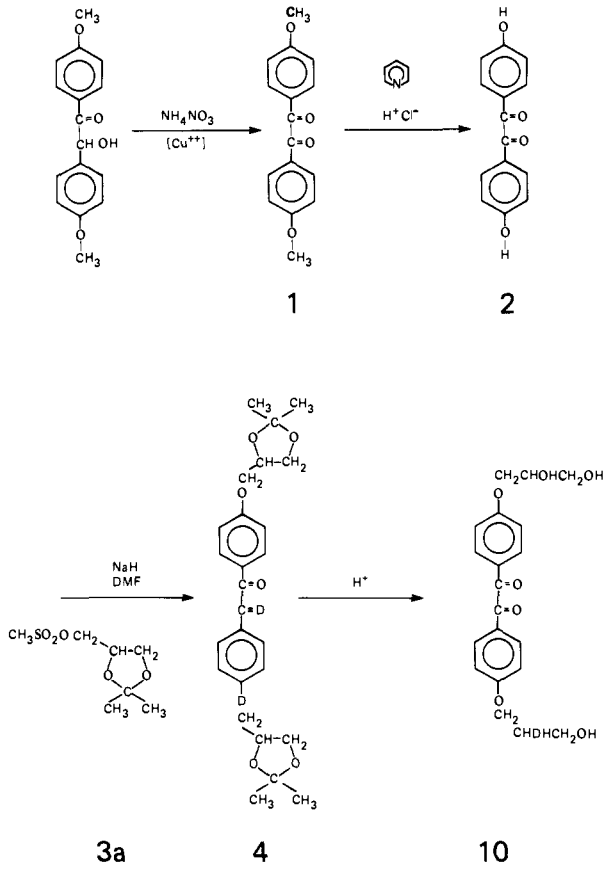

solution NMR, we concluded that we had effected a separation of racemic and meso diacetonide, with a 55% recrystallized overall yield of **4a** and a 17% recrystallized yield of **4b**.

The colors of our compounds together with the earlier data[3] revealed that in the crystalline state, benzils are yellow when small para-substituents (H,OCH_3) are present and nearly colorless when larger substituents ($OC_2H_5,OCH_2(C_5H_9O_2)$) are present. We wished to understand the packing interactions which led to this result. Furthermore, it appeared pertinent to examine similar structural questions for the chiral glyceryl diacetonide, **4c**, available via Scheme I from chiral acetonide mesylate, prepared according to literature methods.[19-22]

We prepared 4,4′-diethoxybenzil (**6**)[23] and 4-ethoxybenzil (**7**)[24] in addition to **4a**, **4b**, and **4c**. Crystal structures of these model compounds and of anisil (**1**), as well as those of the three diacetonides were determined. Together with the published structures of 4,4′-dinitrobenzil (**8**) and benzil (**9**), these data afford previously inaccessible insights into the relationship between

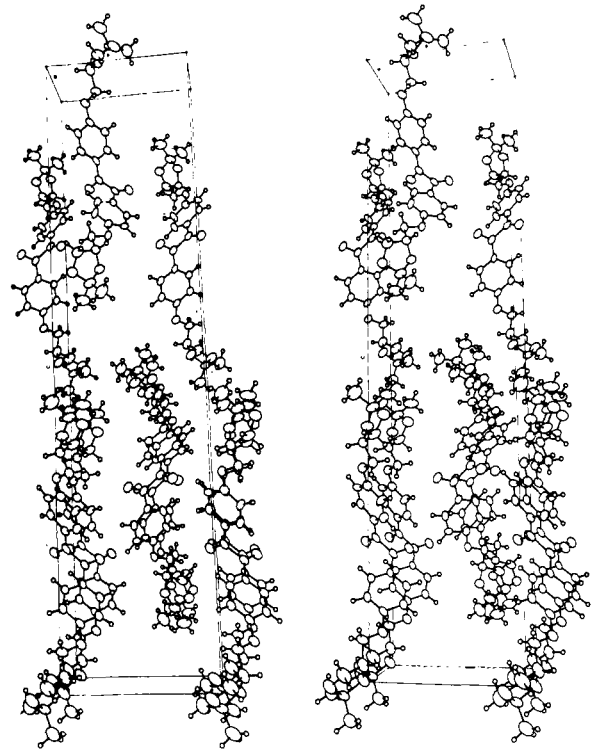

Figure 6. Stereoscopic ORTEP drawing of the unit cell of chiral bisketal benzil approximately along *a*. Direction of *b* is →.

molecular structure and crystal packing in this important class of *p,p′*-disubstituted benzils. The results of these X-ray determinations are summarized in Table I. The angle between the two carbonyls viewed along the intercarbonyl bond is designated τ. Stereo ORTEP views of the unit cells of **1**, **6**, **7**, **4a**, **4b**, and **4c** are shown in Figures 1–6.

The structures can generally be divided into three different sets based on gross packing arrangements: (I) benzil, with chiral, helical chains around the threefold axis; (II) substituted benzils which are stacked directly over each other in alternating centrosymmetrically arrayed sheets; and (III) an intermediate case in which pairwise interactions dominate the close range order while several features of the centrosymmetrically disposed stacks as well as overall centrosymmetry are maintained.

The Class II structures are the chief focus of our interest in this work. We will seek to fit the Class III structures included in this study into the framework within which the Class II structures are analyzed. The Class I structure has been extensively discussed in previous literature although some new insight will be provided into the way in which it arises out of pairwise interactions similar to those which afford the achiral structures of Class III.

Compounds **1**, **4a**, and **6** are members of Class II. All stack in sheets with the essentially planar benzoyl groups twisted at an angle τ to each other, with the tilted groups lying directly over each other in each stack. The unit cell of **4c**, while chiral rather than centrosymmetric, contains similarly disposed sheets of stacked molecules. For this reason we consider **4c** as a member of Class II. Side views of each of these compounds are shown in Figure

(19) Baer, E. *J. Am. Chem. Soc.* **1945**, *67*, 3.
(20) LeCocq, J.; Ballou, C. E. *Biochemistry* **1964**, *3*, 976.
(21) Snowden, J. C.; Fischer, H. O. L. *J. Am. Chem. Soc.* **1941**, *63*, 3244.
(22) Howe, R. J.; Malkin, T. *J. Chem. Soc.* **1951**, 2663.
(23) Vorlander, D. *Ber.* **1911**, *44*, 2455.
(24) Tiffeneau, M.; Levy, J. *Bull. Soc. Chim.* **1931**, *49*, 725.

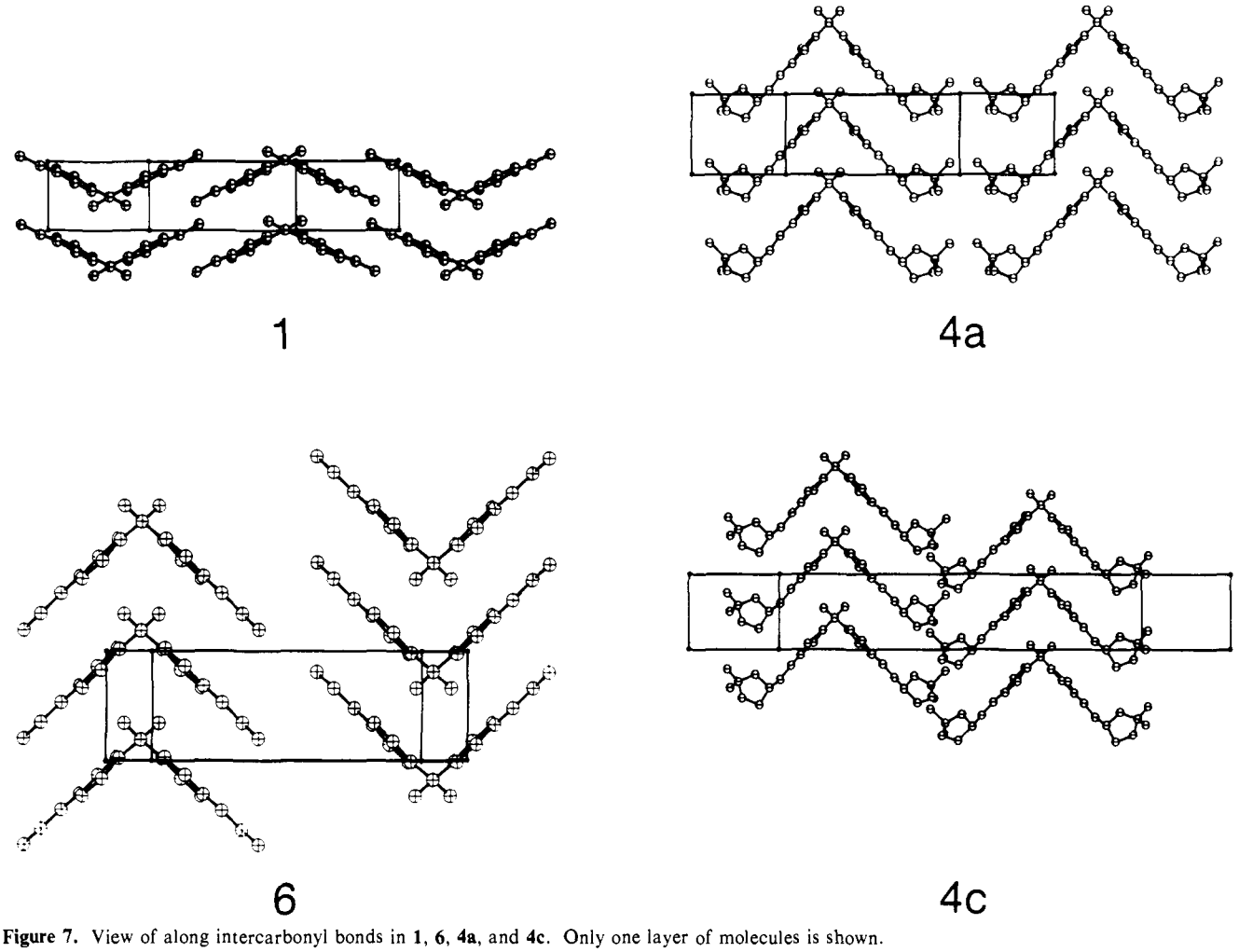

Figure 7. View of along intercarbonyl bonds in **1**, **6**, **4a**, and **4c**. Only one layer of molecules is shown.

Table II. Interplanar Phenyl Ring Spacing in Substituted Benzils

compound	spacing, Å	
1	3.60	
6	3.44	
4a	3.60	
4c	3.77	
7	3.55	3.70
4b	3.29	
8	3.50	3.47
9	3.76	av (3.94, 3.57)

7. The ORTEP[25] plot is shown for the side view of only one sheet of molecules in order to facilitate visualization of the intrastack relationships.

Examination of these side views shows the interplanar distance between the benzene rings to be approximately constant within the set of four structures (Table II). On the other hand, the intrastack distances between corresponding atoms in the substituent groups, i.e., substituent atoms which lie directly over each other and project into each other down the molecular stack, cannot be the same in going from the methyl group to ethyl to dioxacyclopentylmethyl. These groups increase in size as one proceeds through the series.

It appears that van der Waals forces involved in closest packing arrangements account for the variations in stacking throughout the series. This may be explained by reference to Figure 8, which contains schematic representations of the side views of three molecular dispositions. For (a), the trans-planar arrangement is depicted, even though this structure cannot be achieved in the benzils due to peri interactions between carbonyl oxygen and ortho hydrogen of the other phenyl group.[8] This arrangement can in principle accommodate the substituents if their van der Waals thickness is equal to or less than that of the benzoyl group. In (b), a relatively small bending of the molecule out of the planar configuration results in room to accommodate larger substituents. In the figure this is indicated by the increased distance between the circles with the same diameter as in (a) representing the substituent locations on the molecules. Finally, in (c), the largest

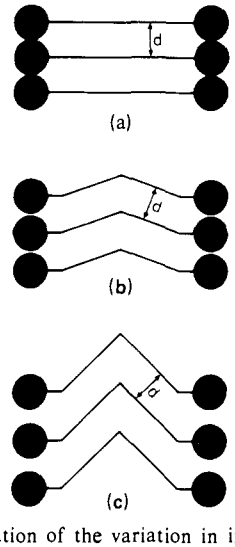

Figure 8. Representation of the variation in interatomic spacing of molecular substituents with variation in intracarbonyl angle at constant phenyl group interplanar spacing.

(25) Johnson, C. K., ORTEP Report ORNL-3794. Oak Ridge National Laboratory, Oak Ridge, TN, 1965.

Table III. Carbonyl Phenyl Ring Dihedral Angles in Substituted Benzils

compd	dihedral angle, deg
1	4.21
6	3.61
4a	3.98
4c	5.64, 8.43
7	3.55, 5.58
4b	4.72, 6.12
8	1.38, 2.24
9	4.77

Table IV. Solution Long Wavelength Spectral Properties of Benzils

compd	λ	ε	ref
1	298	4.35	3
6	300	4.51	3
7	292	4.32	3
4a	296	4.20	this work
4b	296	4.40	this work
4c	298	4.60	this work
8	273	4.10	this work
9	259	4.31	3

substituent thickness which can be accommodated in this packing arrangement is achieved in a molecule in which the benzoyl groups lie at 90° to each other.

In this series of compounds, the change in configuration from anisil, in which the carbonyls are fairly close to coplanar, to the orthogonal disposition of the racemic diacetonide is achieved by the twisting of the carbonyl groups around the central carbon–carbon bond. The benzoyl groups remain relatively planar, each system displaying a small departure from the coplanarity of the carbonyl and benzene ring, as shown in Table III. It thus appears that the intrastack crowding of the para substituents on the benzil molecule forces a twisting of the carbonyls in a system which is attempting to pack as closely as possible while maintaining this basic packing mode. In this indirect manner, the increasing size of the relatively remote substituent leads to decreasing interaction between the two carbonyls and thereby to a blue shift in their absorption spectrum in the solid state. On the other hand, as observed experimentally, in solution, all these molecules are free to rotate to very closely the same intercarbonyl angle and display approximately the same color. Solution spectral characteristics are shown in Table IV.

The molecules in Class III, **7**, **4b**, and **8**,[26] are not stacked in sheets in which each molecule projects directly into the molecule below it in the stack. In the case of **7** the stacking is in columns of noninteracting (quite distant) molecules which project into each other down the (*c*) axis. The main interactions are between similar pairs of phenyl rings (unsubstituted or substituted) in adjacent centrosymmetrically arrayed stacks. An interesting consequence of the packing of this molecule in the unit cell is that the two carbonyls, in addition to the differences arising from the ethoxy or hydrogen on the respective phenyl rings, exist in quite different local environments. One set of carbonyls points approximately down the long nonstacking (*b*) axis while the other carbonyl projects into the interstack space in the direction generally of the short (*a*) axis and toward the ethoxy group of a molecule in another stack (Figure 9).

The stacking of the dinitrobenzil, **8** (not shown)[16] is quite similar in that stacks of moleculers project down the shortest (*c*) axis into each other while the dominant interactions are dipolar in nature and occur between pairs of nitrophenyl carbonyl groups in adjacent stacks. The nitro group of one molecule lies over the oppositely directed phenyl ring of another molecule. Here packing of the molecules in the unit cell enforces a different environment on each

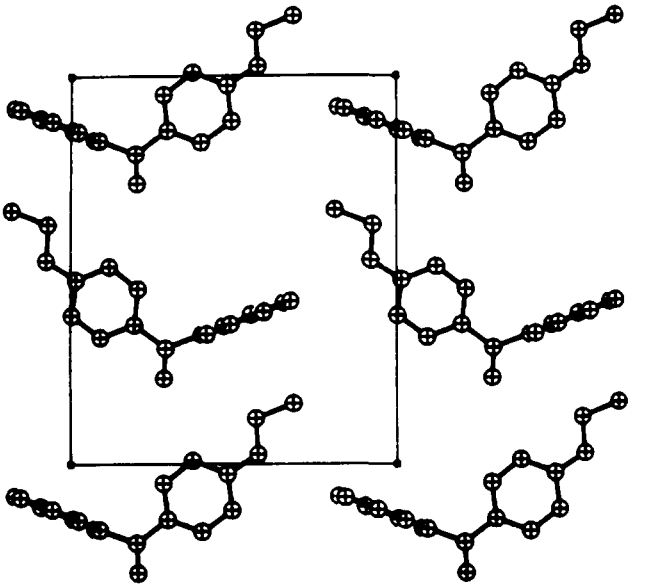

Figure 9. View of monoethoxy benzil approximately perpendicular to *bc* plane. Direction of *b* is →. Only one layer of molecules is shown.

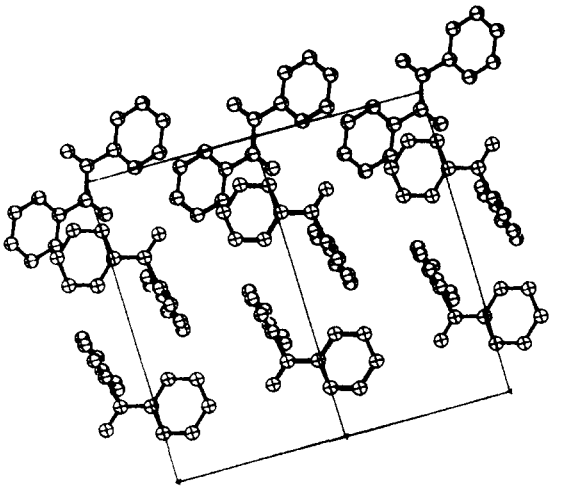

Figure 10. View of benzil down [110] showing nearly parallel placement of phenyl rings averaging 3.77 Å separation.

of the four N–O bonds as well as on each of the two carbonyls, even though, unlike **7**, the two ends of the molecule are the same. The density of **8**, 1.42 g/cm^3, is 3% lower than that of the similarly packed bis(4-nitrophenyl)ketone, 1.46 g/cm^3.[27,28]

The meso bis-ketal, **4b**, is yet another substituted benzil in which there are not closely packed stacks or sheets of molecules. Rather, the stacking down the (*b*) axis is of sheets of molecules slipped along their long axis, the (*a*) axis of the unit cell. In the crystal structure the molecules oscillate between two positions whose long axes make a small angle, perhaps 5–10° with each other. This mode of packing allows for close pairwise interactions between one phenyl ring of each molecule and a more distant packing for the other phenyl ring. Of the molecules whose structures are reported here, this is the only one in which only one of the two phenyl rings is close and parallel to another phenyl ring. As for **7** and **8** the packing of **4b** results in two quite different environments for the carbonyls. For this crystal structure, this difference has been demonstrated by solid state NMR resulting in a remarkable multiplicity in the ^{13}C NMR spectrum.[30] It is inter-

(26) Professor D. Y. Curtin has directed our attention to two additional pertinent crystal structures: 2,2′-pyridil, Hirokawa, S.; Ashida, T. *Acta Cryst.* **1961**, *14*, 774, and 1-phenyl-2(2-pyridyl)ethanedione: Ashida, T.; Hirokawa, S.; Okaya, Y. *Acta Cryst.* **1966**, 506, which are members of Class III.

(27) Chiari, G.; Taylor, H. C. R.; Fronczek, F. R.; Newkome, G. R. *Acta Cryst.* **1980**, *B36*, 2488.

(28) The reported density of **8**, 1.861[16] is in error.

(29) The structures of **1**, **4a**, **4c**, **6**, and **7** were determined by the crystallographic staff of Molecular Structure Corporation, College Station, TX: M. W. Extine, B. A. Frenz, R. A. Meisner, and J. M. Troup.

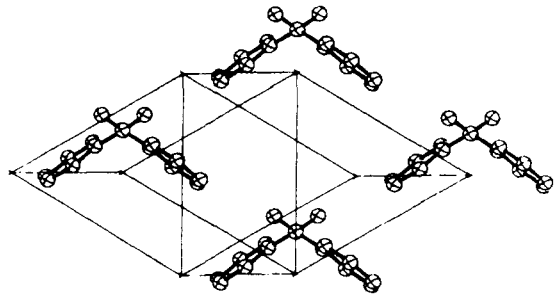

Figure 11. View of one sheet of benzil molecules along the intracarbonyl carbon–carbon bonds. Parallel phenyl planes are separated by 6.59 Å.

esting that the two interacting rings are substituted with dioxacyclopentylmethyl groups of opposite chirality. These interactions combined with the oscillating position of the molecular axis which carries the sterically demanding dioxolanyl groups out of interference with each other lead to a density for the meso compound which is the greatest shown by any of the three diacetonides, 4% larger than that of the chiral and 2% greater than that of the racemic forms.

In benzil none of the closely spaced phenyl rings are parallel to each other. The important interactions in addition to those between each carbonyl and three different carbon–hydrogen pairs in three adjacent columns are pairwise ones between phenyl rings in different benzil molecules. These rings are inclined at an angle of 8° to each other and are separated on the average by 3.77 Å (Figures 10 and 11). This is similar to the greatest distance shown between parallel rings, 3.76 Å, the distance separating parallel phenyl rings in 4c, the chiral bis-ketal. The densities of **4c** and **9** are both 1.26, the lowest value observed in the series. Apparently the 111° angle between the benzoyl groupings in benzil guides the interacting phenyl rings to a 120° rotation between molecules down each trigonal axis. This chiral arrangement must pack with greater density when all the columns are of the same chirality since the alternate mirror plane packing is not observed. Very approximate calculations for a centrosymmetric packing of benzil similar to that of anisil, **1**, suggest a density of 1.21, 4% lower than that observed for the chiral structure. On the other hand, the methoxy groups of anisil would sterically prohibit the combination of interstack and intercolumnar interactions observed in benzil, even though the angle between the benzoyl groups is 124°, quite close to 120°.

In summary, we have prepared and characterized the meso, chiral, and racemic forms of a new masked 4,4′-diglyceryloxy benzil. The crystal structures of six substituted benzils have been reported along with our analysis of their packing modes. There are at least three general packing modes for benzils, which tend to be dominated by van der Waals close packing considerations and the preference for aligning substituted phenyl rings parallel to each other at about 3.45–3.70 Å separation. Our results afford semiquantitative support for earlier recognition that the solid-state color of dicarbonyl compounds is red-shifted by increased overlap and blue-shifted by decreased overlap of the carbonyls. In the case of sheets of stacked substituted benzils, the increased size of the remote substituent is accommodated in the stack by increased twisting of carbonyls while maintaining the closely packed phenyl rings. The molecules we have studied possess different interactions than those predominant in benzil, in view of the fact that both donor and acceptor substituents, and in one case, a chiral substituent, do not lead to structures analogous to that of the simpler compound. We believe that the absence of steric interference on the phenyl rings of benzil together with the inclination of the phenyl rings at an angle close to 120° guides these molecules into an interaction in which chiral trigonal packing is more dense than achiral packing across a mirror plane. It seems likely that packing analogous to Class II or Class III could be displayed by benzil under other conditions of temperature and pressure.

(30) Crowley, J. I.; Fleming, W. W.; Lyerla, J. R.; Yannoni, C. S., to be published; Yannoni, C. S. *Acc. Chem. Res.* **1982**, 201.

Experimental Section

General Considerations. Microanalyses were performed by Chemical Analytical Services, University of California at Berkeley. Melting points were determined on a Reichert MP apparatus. NMR spectra were recorded on a Varian T-60 instrument and infrared spectra employed a Perkin-Elmer 283 instrument. Optical rotations were determined on a Perkin-Elmer 241 MC Polarimeter. Visible and UV spectra were recorded on a Cary 17D. Anisil, Solketal, and D-mannitol were purchased from Aldrich and used without further purification. Monoethoxybenzil and 4,4′-diethoxybenzil were prepared by catalytic oxidation of the corresponding benzoins[31] prepared according to the literature. Literature methods were also employed in the preparation of 4,4′-dinitrobenzil.[16] Microanalyses were satisfactory for all compounds.

(*RS*)-2,2-Dimethyl-1,3-dioxacyclopentyl-4-methyl Mesylate (3a). A 2-L 3-neck round-bottom flask was charged with 264 g (2.0 mol) of Solketal (Aldrich) (**5a**), 412 mL of triethylamine (1.5 mol), and 1.0 L of CH_2Cl_2. The mixture was cooled to 0 °C under argon. Methanesulfonyl chloride, 150 mL (228 g, 2 mol), was carefully added dropwise, while the temperature was kept below 10 °C. During the addition a white precipitate formed which eventually turned yellow. After the addition was completed, the reaction was allowed to stir for 15 min. Water was then added slowly. Following 5 min of additional stirring the solutions were clear and colorless. The organic layer was separated and washed twice with 10% HCl and saturated $NaHCO_3$. Drying over Na_2SO_4 and evaporation of solvent on the Rotavap gave a yellow oil. Distillation (bp 110–112 °C/2 mm) gave 215 g of pure mesylate (1.05 mol, 52%). NMR ($CDCl_3$) δ 1.35 and 1.45 (s, 3 H each, ketal dimethyl), 3.05 (s, 3 H, mesylate), 3.6–4.4 (m, 5 H).

(*R*)-2,2-Dimethyl-1,3-dioxacyclopentyl-4-methyl Mesylate (3c). D-Mannitol was converted to its 1,2,5,6-diacetonide[19] which was oxidatively cleaved to the aldhyde with periodate, and finally reduced with $NaBH_4$ to chiral Solketal (1,2-*O*-isopropylidene-L-glycerol)[20] (**5c**). Chiral solketal was converted to its mesylate (3c) as previously described.[21,22]

Meso and Racemic Di(4-oxyphenyl-2′,2′-dimethyl-1′,3′-dioxacyclopentyl-4′-methyl)ethanedione-1,2 (4a, 4b). Sodium hydride (50% dispersion, 19.83 g, 413 mmol) was placed in a 1-L 3-neck round-bottom flask fitted with a condenser, serum cap, mechanical stirrer, and argon balloon. The hydride was washed twice with pentane to remove the oil. DMF, 500 mL (previously dried over 4A molecular sieves) was added and the suspension was stirred rapidly. Dihydroxy benzil (50 g, 206.6 mmol) in 50 mL of dry DMF was added dropwise over 10 min. The hydrogen produced during this addition was allowed to escape. The thick yellow-green paste was stirred at room temperature for 30 min. Solketal mesylate (**3a**) (120 g, 571 mmol) was added neat. The reaction mixture was heated at 100 °C for 18 h. The resulting low viscosity dark solution was carefully poured into 3 times its volume of cold water with rapid stirring. A light orange precipitate separated and was collected by filtration on a sintered glass filter. After three water washes, the solid was dried in a vacuum oven and triturated with 15–20 times its weight of acetone. This treatment removed most of the yellow color. The resulting white solid was recrystallized from acetone or toluene to afford 54 g of **4a** (55.6%). NMR ($CDCl_3$) δ 1.4 and 1.45 (two s, 3 H each, ketal dimethyl), 3.0–4.7 (m, 10 H, CHO, CH_2O), 7.0 and 7.95 (d, J = 8 Hz, 4 H each, aromatic). IR (KBr) 1665, 1600, 1570, 1250, 1215, 1160, 1070, 1045 TLC (20% ethylacetate/benzene on silica gel) R_f = 0.4, mp ~165 °C.

Upon rotavaporation of the mother liquor from acetone trituration of the bisketal product, a low melting solid was obtained which almost completely dissolved in acetone during a second attempted trituration. Rotavaporation again afforded a low melting solid, or in some cases, an oil which could be recrystallized at low temperatures (−20 °C) from toluene or acetone/hexane. While this material had essentially identical UV, solution NMR, and IR to the earlier isolated **4a**, its melting point was different, 116 °C. The yield of crystallized **4b** was 17%. Recycling mother liquors resulted in additional **4a** and **4b**, although 8% of the original crude product was not recovered.

(*SS*)-Di(4-oxyphenyl-2′,2′-dimethyl-1′,3′-dioxacyclopentyl-4′-methyl)ethanedione-1,2 (4c). The chiral glycerol acetonide was used to prepare the chiral **4c** according to the same procedure used to obtain the racemic/meso mixture. NMR, IR, and TLC were identical. $[\alpha]^{20}_D$ = +15°.

Crystal Structure Determination

Data Collection. Crystals were grown by cooling or evaporation from the tabulated solvents as indicated. Crystals of dimensions tabulated below were mounted on glass fibers. The long axis of each needlelike crystal was positioned with its long axis parallel to the φ axis of the

(31) Weiss, M.; Appel, M. *J. Am. Chem. Soc.* **1948**, *70*, 3666.

goniometer; a platelike crystal of **4c** was mounted with its shortest axis orthogonal to the ϕ axis of the goniometer. Preliminary examination and data collection were performed with Cu Kα radiation (λ = 1.54184 Å) on an Enraf-Nonius CAD4 computer controlled κ axis diffractometer equipped with a graphite crystal incident beam monochromator except in the case of **4b**.

Cell constants and an orientation matrix for data collection were obtained from least-squares refinement of the setting angles of 25 reflections, measured using the computer controlled diagonal slit method of centering. Primary crystal structure data are shown in Table I. As a check on crystal quality, ω scans of several intense reflections were measured; the width at half height was as indicated in Table V (Supplementary Material) with a take-off angle of 2.8°, indicating good crystal quality in each case. From the systematic absences, also tabulated, and from subsequent least-squares refinement, the space groups were determined.

The data were collected at a temperature of 23 ± 1 °C using the ω-scan technique (Table VI, Supplementary Material). The scan rate varied from 2 to 2θ/min (in ω). The variable scan rate allows rapid data collection for intense relfections where a fast scan is used and assures good counting statistics for weak reflections where a slow scan rate is used. Data were collected to a maximum 2θ value as indicated. The scan range (in degrees) was determined as a function of θ to correct for the separation of the Kα doublet; the scan width was calculated as follows.

$$\theta \text{ scan width} = \omega \text{ scan width} = A + B \tan \theta$$

Values of A and B are tabulated. Moving-crystal moving-counter background counts were made by scanning an additional 25% above and below this range. Thus the ratio of peak counting time to background counting time was 2/1. The counter aperture was also adjusted as a function of θ. The horizontal aperture width ranged between the tabulated values, and the vertical aperture was set at a value which also appears in the table. The diameter of the incident beam collimator was 0.7 mm and the crystal to detector distance was 21 cm. For intense reflections, except in the case of 6, a Ni foil attenuator was automatically inserted in front of the detector; the attenuator factor is 15.5 for **1**, **4a**, and **4c** and 15.8 for **7**.

Data Reduction. Reflections were collected to the extent tabulated in Table VI; a portion of these, also tabulated, are unique and not systematically absent. In the case of **4c**, Friedel equivalent reflections were collected. As a check on crystal and electronic stability, three representative reflections were measured at the tabulated time intervals. The intensities of these standards remained constant within experimental error throughout data collection.

Lorentz and polarization corrections were applied to the data. The linear absorption coefficient is tabulated for each structure determination for Cu Kα radiation. No absorption correction was made. An extinction correction was not necessary.

Structure Solution and Refinement. Each structure was solved by direct methods. Using reflections whose number and minimum E is tabulated, and 2000 relationships, a total of 16 phase sets were produced. All nonhydrogen atoms were located from an E-map prepared from the phase set with probability statistics, the absolute figure of merit and residual values of which are tabulated. For **1**, **4a**, **6**, and **7**, hydrogen atoms were located and their positions and isotropic thermal parameters refined. For **4b**, hydrogen atoms were not located or calculated for the refinement. For **4c**, hydrogen atoms (in calculated positions) were added to the structure factor calculations but their positions were not refined. Hydrogen atom positions were calculated assuming idealized geometries with C–H bond distances of 0.95 Å. This compound was refined as the LL enantiomer, which is known to be correct from the method of synthesis. All structures were refined in full-matrix least squares where the function minimized was $\sum\omega(|F_o| - |F_c|)^2$ and the weight w is defined as $4F_o^2/\sigma^2(F_o^2)$.

The standard deviation of the intensities, $\sigma(F_o^2)$, is defined as

$$\sigma^2(F_o^2) = [S^2(C + R^2B) + (pF_o^2)^2]/L_p^2$$

where S is scan rate, C is total integrated peak count, R is ratio of scan to background counting time, B is the total background count, L_p is the Lorentz-polarization factor, and the parameter p is a factor introduced to downweight intense reflections, here set at 0.050. Scattering factors,[32] anomalous dispersion effects included in F_c,[33] and the values for $\Delta f'$ and $\Delta f''$[34] are from the literature. Only reflections having intensities greater by some enhancement factor than their standard deviation were used in the refinements; this ratio is listed in Table IV. The final cycle of refinement converged (largest parameter shift was considerably less than one esd) with unweighted and weighted agreement factors of

$$R_1 = \sum||F_o| - |F_c||/\sum|F_o|$$

and

$$R_2 = \sqrt{(\sum w(|F_o| - |F_c|)^2/\sum wF_o^2)}$$

The number of variable parameters used, the ratios of intensity to standard deviation and of maximum parameter shift to esd together with R_1 and R_2 and the standard deviation of an observation of unit weight are tabulated. The final difference Fourier maps showed no significant residual electron density. Plots of $\sum w(|F_o| - |F_c|)^2$ vs. $|F_o|$, reflection order in data collection, sin θ/λ and various classes of indices showed no unusual trends.

These calculations were performed on linked PDP-11/45-11/60 computers using the Enraf-Nonius Structure Determination Package[35] as well as private programs of Molecular Structure Corporation.

Acknowledgment. It is a pleasure to acknowledge the constructive reading of this manuscript by our colleagues, Dr. Linda Nebenzahl and Dr. Grant Willson, and to acknowledge their assistance in improving the presentation of our results.

Registry No. 1, 1226-42-2; **2**, 33288-79-8; (±)-**3a**, 34331-40-3; (±)-**3a**-ol, 22323-83-7; **3c**, 83461-40-9; **4a**, 86971-11-1; **4b**, 86971-10-0; **4c**, 87038-34-4; **5c**, 22323-82-6; **6**, 2132-59-4; **7**, 39229-13-5; **8**, 6067-45-4; **9**, 134-81-6; methanesulfonyl chloride, 124-63-0; D-mannitol, 69-65-8; D-mannitol 1,2:5,6-diacetonide, 1707-77-3.

Supplementary Material Available: Complete listing of crystal data for substituted benzils, Table V, collection and processing data for substituted benzils, Table VI, complete listing of positional and thermal parameters, bond lengths and bond angles and their estimated standard deviations, Tables VII–XIV, general temperature factor expressions, B'S, Tables XV–XIX, general temperature factor expressions, U's, Tables XX–XIV, root mean square (rms) amplitudes of thermal vibrations, Tables XXV–XXIX, torsional angles, Tables XXX–XXXIV, weighted least-squares planes, Tables XXXV–XXXIX, and experimental and calculated structure factors (Tables XL–XLIV). In addition, Figure 12 displays the numbering system used in Tables VII–XIX (a) for **1**, **4a**, and **6**, (b) for **7**, and (c) for **4b** and **4c** (91 pages). Ordering information is given on any current masthead page.

(32) Cromer, D. T.; Waber, J. T. "International Tables for X-Ray Crystallography", Vol. IV; The Kynoch Press: Birmingham, England, 1974; Table 2.2B.
(33) Ibers, J. A.; Hamilton, W. C. *Acta Cryst.* **1964**, *17*, 781.
(34) Cromer, D. T. "International Tables for X-Ray Crystallography", Vol. IV; The Kynoch Press: Birmingham, England, 1974; Table 2.3.1.
(35) Frenz, B. A. In "Computing in Crystallography"; Schenk, H.; Olthof-Hazekamp, R.; van Konigsveld, H.; Bassi, G. C., Ed.; Delft University Press: Delft, Holland, 1978; pp 64–71.

Measurements of Molecular g Values, Magnetic Susceptibility Anisotropies, and Quadrupole Moments for the Acetylene–HCl Complex

S. G. Kukolich,*† W. G. Read,* J. A. Shea,* and E. J. Campbell*

Contribution from Noyes Chemical Laboratory, University of Illinois, Urbana, Illinois 61801. *Received April 11, 1983*

Abstract: Rotational transitions for acetylene–HCl were measured in magnetic fields of 28 and 30 kG using a pulsed-nozzle, Fourier transform microwave spectrometer. Measured molecular g values are $g_{aa} = 0.0519$ (5), $g_{bb} = -0.0006$ (2), and $g_{cc} = 0.0025$ (2). Susceptibility anisotropies are $2\chi_{aa} - \chi_{bb} - \chi_{cc} = 0.08$ (4) $\times 10^{-9}$ and $2\chi_{bb} - \chi_{cc} - \chi_{aa} = -1.14$ (8) $\times 10^{-9}$ MHz/G^2. Molecular quadrupole moments for the complex are $Q_{aa} = -2.6$ (3), $Q_{bb} = 6.2$ (3), and $Q_{cc} = -3.7$ (3) $\times 10^{-26}$ esu cm^2. We find that the molecular g value for acetylene is positive, $g_\perp = 0.044$ (1). The molecular quadrupole moment of acetylene is found to be 8.0 (16) $\times 10^{-26}$ esu cm^2 in good agreement with calculated values.

I. Introduction

Microwave rotational spectra for the acetylene–HCl complex were reported by Legon, Aldrich, and Flygare.[1] This is a planar T-shaped complex with bonding of the HCl proton to the π electrons of acetylene. A series of π-bonded complexes involving acetylene, ethylene, or cyclopropane bonded to HF, HCl, or HCN have been studied using the Flygare–Balle pulsed beam spectrometer system.[2,3] The spectrometer for Zeeman measurements on complexes was described earlier.[4,5] The present Zeeman measurements on acetylene–HCl were done primarily to obtain information on the electronic structure of acetylene. It was demonstrated in other work[6] that molecular Zeeman parameters for complexes could be accurately obtained from Zeeman parameters for the substituent monomers. The Zeeman parameters of interest here are molecular g values, magnetic susceptibility anisotropies, and molecular quadrupole moments. Measurements of the molecular Zeeman effect for a large number of stable molecules have been reported by Flygare and co-workers and other groups. Reviews of this earlier work have been published.[7] These measurements provide data on quadrupole moments for the charge distribution in molecules and both paramagnetic and diamagnetic contributions to magnetic susceptibility tensors.

Molecular g values, susceptibility anisotropies, and the molecular quadrupole moments were obtained from Zeeman measurements on the acetylene–HCl complex. These values for the complex are used with previously measured parameters for HCl[8] to obtain susceptibility anisotropies and molecular quadrupole moments for acetylene.

II. Experimental Section

A sensitive high-resolution Fourier transform microwave spectrometer was developed[2,3] for the study of weakly bound complexes. A similar spectrometer[4-6] was developed for Zeeman studies using a smaller cavity placed in a superconducting solenoid magnet. This spectrometer is described in reports on ArHF[4] and ArHCl.[5] In the present experiments the magnetic field is perpendicular to the microwave electric field so $\Delta M_F = \pm 1$ transitions are observed. The total angular momentum is $F = I_{Cl} + J$. A gas mixture of 2% HCl and 2% acetylene in argon at 1.5 atm pressure was prepared in a 1-L tank. The gas was pulsed into the microwave cavity using a modified Veeco PV-10 piezoelectric valve. Following the gas pulse a microwave pulse was sent into the cavity; this produced a molecular emission signal which was detected and amplified using a gated superheterodyne receiver. The time domain molecular emission signal was digitized, averaged, and Fourier transformed to obtain the frequency spectrum. Each frequency setting of the microwave oscillator gives an effective bandwidth of about 0.5 MHz so a number of spectra were taken in the region where lines are expected. Fourier transforms are obtained using an LSI-11 computer. Magnetic fields used in these experiments were 28 113 and 30 098 G. The Zeeman splitting of the $J = 0 \rightarrow 1$ transition of OCS was used to calibrate the field. Measured spectra for $\Delta M = \pm 1$, $J = 1 \rightarrow 2$ transitions in the acetylene–HCl complex are shown in Figure 1. Results of the measurements are given in Table I.

III. Data Analysis

The Hamiltonian used to analyze the data contains terms due to the rotational energy (A, B, C are rotational constants; D_J, D_{JK} are distortion constants), the molecular g values (g_{gg}), the magnetic susceptibility anisotropies ($\chi_{gg} - \bar{\chi}$), nuclear quadrupole coupling of ^{35}Cl (eQq_{gg}), and magnetic moment and shielding anisotropies ($\sigma_{gg} - \bar{\sigma}$) of ^{35}Cl. The Hamiltonian, $\mathcal{H}$, is given in eq 1.

$$\mathcal{H} = AJ_a^2 + BJ_b^2 + CJ_c^2 - D_J J^2(J+1)^2 - D_{JK}J(J+1)J_a^2 - \mu_N J_z H \sum_g g_{gg}\langle J_g^2\rangle/[J(J+1)] - H^2[3J_z^2 - J(J+1)]\sum_g(\chi_{gg} - \bar{\chi})\langle J_g^2\rangle/[(2J-1)(2J+3)J(J+1)] + [3(\mathbf{J}\cdot\mathbf{I})^2 + 3(\mathbf{J}\cdot\mathbf{I})/2 - \mathbf{J}^2\mathbf{I}^2]\sum_g eQq_{gg}\langle J_g^2\rangle/[2J(2J-1)I(2I-1)(J+1)(2J+3)] - g_I\mu_N(1-\bar{\sigma})I_z H + 2g_I\mu_N I_z H[3J_z^2 - J(J+1)]\sum_g(\sigma_{gg} - \bar{\sigma})\langle J_g^2\rangle/[(2J-1)(2J+3)J(J+1)] \quad (1)$$

The sums are g are taken over the principal axes, $g = a, b, c$. The components of the angular momentum vector $\mathbf{J}$ are taken in the coordinate system with z along the applied magnetic field. No matrix elements off-diagonal in J are included in this analysis. Shifts in transition frequencies due to terms off-diagonal in J would be a few kilohertz or less.

The valus of B, C, D_{JK}, and eQq_{gg} used in the analysis of Zeeman data are determined by fitting zero-field $J = 1 \rightarrow 2$ transitions for acetylene–HCl. A and D_J were taken from original measurements. The values obtained from the original measurements on this complex give a good fit to six rotational transitions, including $J = 1 \rightarrow 2$ and $J = 2 \rightarrow 3$ transitions, but do not give the best possible fit to $J = 1 \rightarrow 2$ transitions alone. This is most likely due to centrifugal distortion effects. Since it is important in analysis of the Zeeman data to reproduce the zero-field lines as accurately as possible, only the $1_{01} \rightarrow 2_{02}$, $1_{11} \rightarrow 2_{12}$, and 1_{10}

† Permanent address: Department of Chemistry, University of Arizona, Tucson, Arizona 85721.

(1) A. C. Legon, P. D. Aldrich, and W. H. Flygare, *J. Chem. Phys.*, **75**, 625 (1981).
(2) T. J. Balle and W. H. Flygare, *Rev. Sci. Instrum.*, **52**, 33 (1981).
(3) T. J. Balle, E. J. Campbell, M. R. Keenan, and W. H. Flygare, *J. Chem. Phys.*, **72**, 926 (1980).
(4) W. G. Read and E. J. Campbell, *Phys. Rev. Lett.* **49**, 1146 (1982).
(5) E. J. Campbell and W. G. Read, *J. Chem. Phys.*, **78**, 6490 (1983).
(6) W. G. Read and E. J. Campbell, *J. Chem. Phys.*, **78**, 6515 (1983).
(7) W. H. Flygare and R. C. Benson, *Mol. Phys.* **20**, 225 (1971); W. H. Flygare "Critical Evaluation of Chemical and Physical Structural Information"; Lide, D. R., Paul M. A., Eds. 1974, p 449; D. H. Sutter and W. H. Flygare, *Top. Curr. Chem.*, **63**, 89 (1976).
(8) F. H. de Leeuw and A. Dymanus, *J. Mol. Spectrosc.* **48**, 427 (1973).

0002-7863/83/1505-6423$01.50/0